Spontaneous Potentials in Hydrocarbon Reservoirs during Waterflooding: Application to Waterfront Monitoring*

M.D. Jackson[1], M.Y. Gulamali[1], E. Leinov[1], J.H. Saunders[1], and J. Vinogradov[1]

Search and Discovery Article #120066 (2012)
Posted December 31, 2012

*Adapted from extended abstract prepared in conjunction with poster presentation at AAPG Hedberg Conference, Fundamental Controls on Flow in Carbonates, July 8-13, 2012, Saint-Cyr Sur Mer, Provence, France, AAPG©2012

[1]Department of Earth Science and Engineering, Imperial College, London, UK (m.d.jackson@imperial.ac.uk)

Abstract

Spontaneous potential (SP) is routinely measured using wireline tools during reservoir characterization [e.g. Schlumberger et al., 1934]. However, SP signals are also generated during hydrocarbon production, in response to gradients in the water phase (i) pressure (relative to hydrostatic), which gives rise to electrokinetic (EK) or streaming potentials, (ii) chemical composition, which gives rise to electrochemical (EC) potentials, and (iii) temperature, which gives rise to thermoelectric (TE) potentials. We use numerical modeling to investigate the likely magnitude of the SP in an oil reservoir during production, and suggest that measurements of SP, using electrodes permanently installed downhole, could be used to detect and monitor water encroaching on a well while it is several tens to hundreds of meters away. We simulate the SP generated during production from a single vertical well, with pressure support provided by water injection. We vary the production rate, and the temperature and salinity of the injected water, to vary the contribution of the different components of the SP signal. We also vary the values of the so-called 'coupling coefficients' which relate gradients in water phase pressure, salinity and temperature, to gradients in electrical potential.

Numerical Modeling

We simulate SP signals in a 3D reservoir model based on that used by (Saunders et al., 2008). A horizontal sandstone reservoir layer contains a single vertical production well and is bounded by shales above, below and laterally on three of the four vertical sides (Figure 1). The shales are water saturated and so electrically conductive, but the water is immobile. The fourth side is bounded by a sandstone layer. These additional parts of the model domain allow us to use the potential at the outer boundary as a reference; numerical tests show

that increasing the size of the domain beyond that used does not affect the results. In reality, the reference would be one or more distant electrodes, which could be located at the surface, or at the well in a shallower rock formation. Rock and fluid properties are typical of many reservoirs (Table 1). Values of the SP coupling coefficients used in the numerical modeling are salinity, temperature and saturation dependent, and are based on relatively sparse published data. The values of these coupling coefficients are a key uncertainty, and further work is required to characterize their values at reservoir conditions.

Results

We begin by simulating a case where oil is produced at a rate of 10,000 bbl/day and brine flows into the reservoir at the same rate with a salinity of 0.5 M and a temperature of 30° C. The reservoir permeability is uniformly 150 mD and the initial temperature and formation brine salinity are 80° C and 1 M respectively. The chosen parameters represent the injection of seawater into a reservoir containing typical saline formation brine. Figure 2 shows data obtained along a 1D profile at the centre of the reservoir layer, oriented parallel to the long axis of the model and passing through the well, for four different time steps. A water saturation front moves towards the well. Ahead of the front, oil flows in the presence of irreducible water; behind the front, water flows in the presence of residual oil. At the front, water saturation varies rapidly over a limited spatial interval. Temperature and salinity fronts also move towards the well; however, these both lag behind the saturation front, because of mixing of the injected and formation brines, and because sensible heat is required to change the temperature of the reservoir rock and fluids.

The pressure gradient in the water phase gives rise to an EK potential, which has a peak at the location of the waterfront and decays toward zero (measured with respect to a distant reference electrode) ahead of and behind the front. The EK potential falls to zero ahead of the front because there is no streaming current associated with the flow of oil, and falls to zero behind the front because the streaming current is constant where the water saturation is constant. The peak EK potential follows the waterfront as it moves through the reservoir, and is associated with the front because the divergence of the streaming current becomes nonzero where the saturation changes, so the waterfront acts as a current source. The salinity and temperature gradients in the water phase also give rise to EC and TE potentials. The TE potential is zero ahead of the temperature front and negative behind the leading edge of the front (measured with respect to a distant reference electrode), reaching a maximum value (in magnitude) at the trailing edge of the temperature front. The EC potential is also zero ahead of the salinity front, but becomes positive behind the leading edge of the front, reaching a maximum value some distance behind the trailing edge of the front.

Figure 3 shows the total SP recorded along the production well within the reservoir interval for each of the time steps shown in Figure 2. The individual EK, EC and TE contributions combine to yield a total SP signal that reaches c. 1.5 mV at water breakthrough (0 days) and exceeds an estimated noise level of 0.1 mV, based on field measurements of SP, approximately 1000 days before breakthrough. At this time, the waterfront is still approximately 250m away from the production well (see the upper panel of Figure 2). Thus, changes in

electrical potential measured at a production well may be indicative of an approaching waterfront while the front is still some distance away from the well.

We now vary the pressure gradient by varying the production rate over the range 1000-20,000 bbl/day and reservoir permeability over the range 75-1500 mD. We also change the salinity gradient by varying the formation brine salinity over the range 0.5 M to 5 M while keeping the injected brine salinity constant at 0.5 M. The SP signal reaches a maximum of 2 mV at the highest production rate (20,000 bbl/day in a 150 mD reservoir) and lowest reservoir permeability investigated (75 mD at a production rate of 10,00 bbl day) and exceeds 0.3 mV even for the lowest value of production rate (1000 bbl/day in a 150 mD reservoir) and highest value of reservoir permeability investigated (1500 mD at a production rate of 10,00 bbl day); the signal therefore comfortably exceeds the estimated noise level of 0.1 mV over the range of reservoir production rates and permeability investigated (Figure 4). However, note that the signal continues to decrease with decreasing production rate or increasing permeability. The TE potential is significantly smaller in magnitude than either the EK or EC potentials and its contribution can be neglected.

We finish by investigating the impact of reservoir heterogeneity on the SP signal at the production well using a simple model in which a high permeability layer of 1500 mD is embedded in a reservoir of 150 mD. The layer is not intersected by the production well, so its presence would likely not be captured in reservoir models, leading to incorrect predictions of water movement during production. Our aim is to determine whether the presence of this layer, and its impact on water movement, could be identified prior to water breakthrough at the well. In a well equipped with inflow control valves, this information would allow proactive control of inflow, to delay or prevent water breakthrough.

Figure 5 shows a cross-section through the homogeneous model showing water saturation at three different times, and the corresponding potentials observed along the production well. The maximum potentials are observed at the centre of the well, even though the water front is flat; this reflects the electrically conductive shales above and below the reservoir. The total SP signal is dominated by the EK and EC potentials. The corresponding data for the heterogeneous reservoir model are shown in Figure 6. The encroaching water exploits the high permeability layers, moving more rapidly through these towards the production well. The resulting SP signals at the well reflect fingering of the waterfront, which could be distinguished on the basis of the SP profile along the well.

Conclusions

These results suggest that waterfronts could be tracked and imaged using downhole measurements of SP at one or more production wells. In wells equipped with inflow control valves, this information would allow proactive control of inflow, to delay or prevent water breakthrough. However, the magnitude of the signal recorded at a well will depend upon a number of reservoir and production parameters, including production rate, reservoir permeability and permeability heterogeneity, formation brine salinity and temperature,

and the coupling coefficients that relate gradients in water phase pressure (relative to hydrostatic), concentration and temperature, to gradients in electrical potential. Consequently, the SP signal will be specific to a given reservoir and production scenario. Moreover, the values of the coupling coefficients are still poorly understood. Future work will need to address three key issues. The first of these concerns the downhole hardware required to acquire SP data during production and transmit these data to surface. The second concerns interpretation of the measured signals for reservoir properties of interest. Our forward models demonstrate that SP signals at a well are sensitive to the location and geometry of an encroaching waterfront; the next step is to develop methods to determine the waterfront location and geometry from the measured signals in conjunction with other reservoir data. The third concerns the nature of the SP coupling coefficients; further laboratory work is required to characterize these at oilfield conditions. Finally, a field trial is required to confirm the modeling results.

Acknowledgments

This work was funded by Shell International Exploration and Production B.V. who are gratefully acknowledged. Schlumberger are thanked for providing the Eclipse 100 simulator.

References

Jaafar, M.Z., J. Vinogradov, and M.D. Jackson, 2009, Measurement of Streaming Potential Coupling Coefficient in Sandstones Saturated with High Salinity NaCl Brine: Geophysical Research Letters, v. 36, L21306, doi: 10.1029/2009GL040549.

Jackson, M.D., 2010, Multiphase electrokinetic coupling: Insights into the impact of fluid and charge distribution at the pore-scale from a bundle of capillary tubes model: J. Geophysical Research, v. 115, B07206, doi:10.1029/2009JB007092.

Jackson, M.D., 2008, Characterization of Multiphase Electrokinetic Coupling Using a Bundle of Capillary Tubes Model: J. Geophysical Research, v. 113, B04201, doi: 10.1029/2007JB005490.

Leinov, E., J. Vinogradov, and M.D. Jackson, 2010, Measurements of thermoelectric coupling coefficient in brine-saturated sandstones: Geophysical Research Letters, v. 37, L23308, doi:10.1029/2010GL045379.

Ortiz Jr., I., J.S. Osoba, and W.D. von Gonten, 1973, Relationship of the Electrochemical Potential of Porous Media with Hydrocarbon Saturation: The Log Analyst, v. 14, p. 25-32.

Reppert, P.M. and F.D. Morgan, 2003, Temperature-dependent streaming potentials: 1. Theory: J. Geophysical Research, v. 108, p. 2546. doi: 10.1029/2002JB001754.

Reppert, P.M. and F.D. Morgan, 2003, Temperature-dependent streaming potentials: 2. Laboratory: J. Geophysical Research, v. 108, p. 2547. doi: 10.1029/2002JB001755.

Revil, A., 1999, Ionic diffusivity, electrical conductivity, membrane and thermoelectric potentials in colloids and granular porous media: A unified model: J. Coll. Interf. Sci., v. 212, p. 503-522.

Revil, A. and A. Cerepi, 2004, Streaming potentials in two-phase flow conditions: Geophysical Research Letters, v. 31, L11605, doi:10.1029/2004GL020140.

Schlumberger, C., M. Schlumberger and E.G. Leonardsen, 1934, A new contribution to subsurface studies by means of electrical measurements in drill holes: Trans. AIME 110, p. 273-282.

Saunders, J.H., M.D. Jackson, and C.C. Pain, 2008, Fluid flow monitoring in oil fields using downhole measurements of electrokinetic potential: Geophysics, v. 73, E165-E180.

Vinogradov J., M.Z. Jaafar, M.D. Jackson, 2010, Measurement of streaming potential coupling coefficient in sandstones saturated with natural and artificial brines at high salinity: J. Geophysical Research, v. 115, B12204, doi: 10.1029/2010JB007593.

Vinogradov, J. and M.D. Jackson, 2011, Multiphase streaming potential in sandstones saturated with gas/brine and oil/brine during drainage and imbibition: Geophysical Research Letters, v. 38, L01301, doi:10.1029/2010GL045726.

Table 1. Rock and fluid properties. Where ranges are shown, the value is varied in a simple sensitivity analysis.			
Property (unit)	Rock	Oil	Water
Viscosity (cP)	-	1	1
Density (kgm^{-3})	2100	1000	1000
Compressibility (bar^{-1})	1×10^{-5}	1×10^{-4}	5×10^{-5}
Specific heat capacity ($J\ kg^{-1}\ °K^{-1}$)	900	2200	4200
Formation (initial) salinity (M)	-	-	0.5 – 5
Injection salinity (M)	-	-	0.5 (approx. seawater)
Formation (initial) temperature (°C)	30-130	30-130	30-130
Injection temperature (°C)	-	-	30
Porosity	0.25	-	-
Permeability (mD)	15 - 1500	-	-
Irreducible water saturation	0.2	-	-
Residual oil saturation	0.2	-	-
End-point water relative permeability	0.3	-	-
End-point oil relative permeability	0.8	-	-

Table 1. Rock and fluid properties. Where ranges are shown, the value is varied in a simple sensitivity analysis.

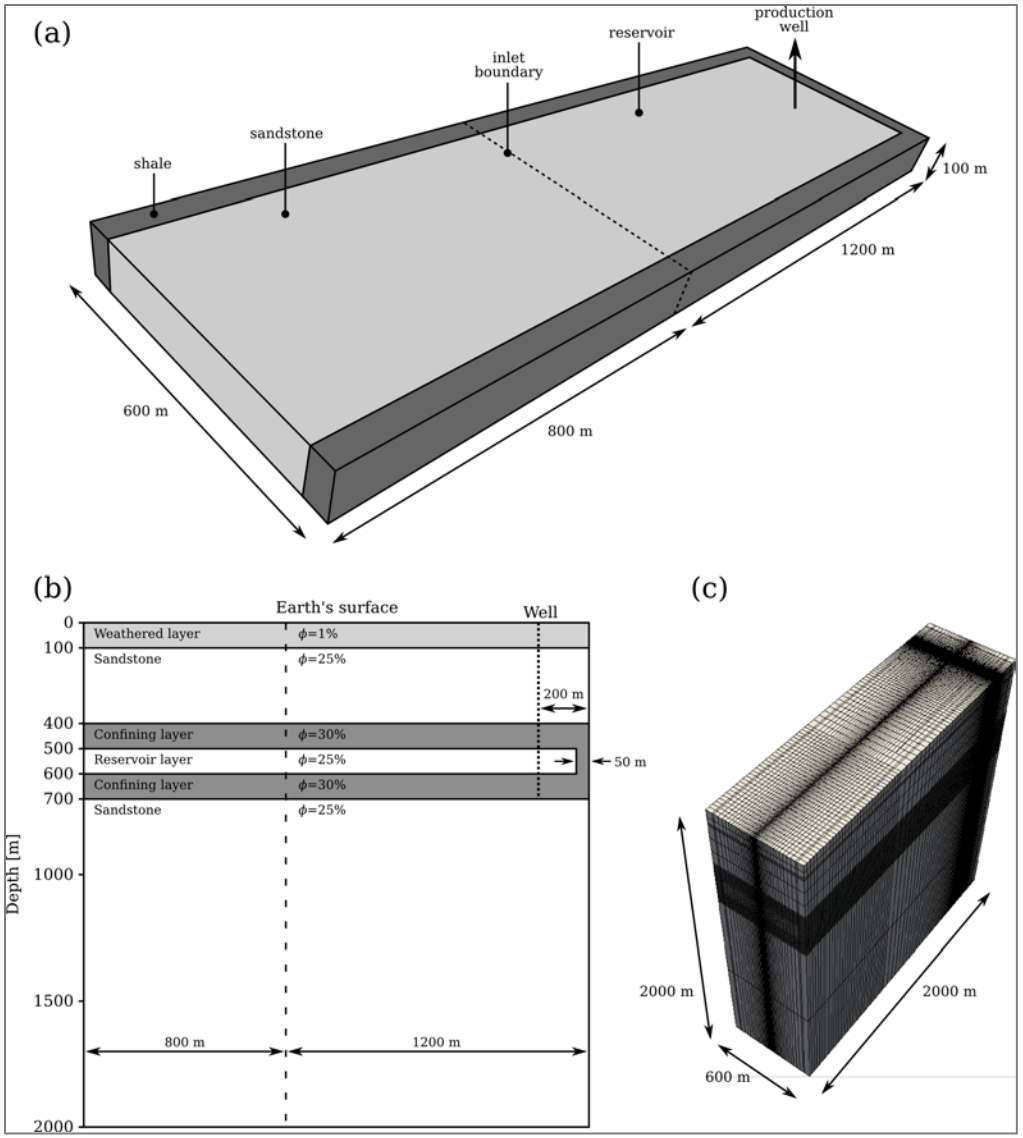

Figure 1. The numerical reservoir model. Water enters the reservoir over the inlet boundary and flows towards the production well; this water is sourced from injection wells which are not explicitly described in the model. The sandstone and shale layers around the reservoir allow us to treat the model boundaries as ‘infinitely’ far away in the electrical problem. (b) Section through the entire model. The reservoir layer, between 500 and 600 m depth, lies between two electrically conductive but impermeable shale layers. Further sandstone layers lie above and below the shales, with a thin weathered layer at the Earth’s surface. c) Grid used for modeling. The location of the well and reservoir layer are indicated by refinement of the grid.

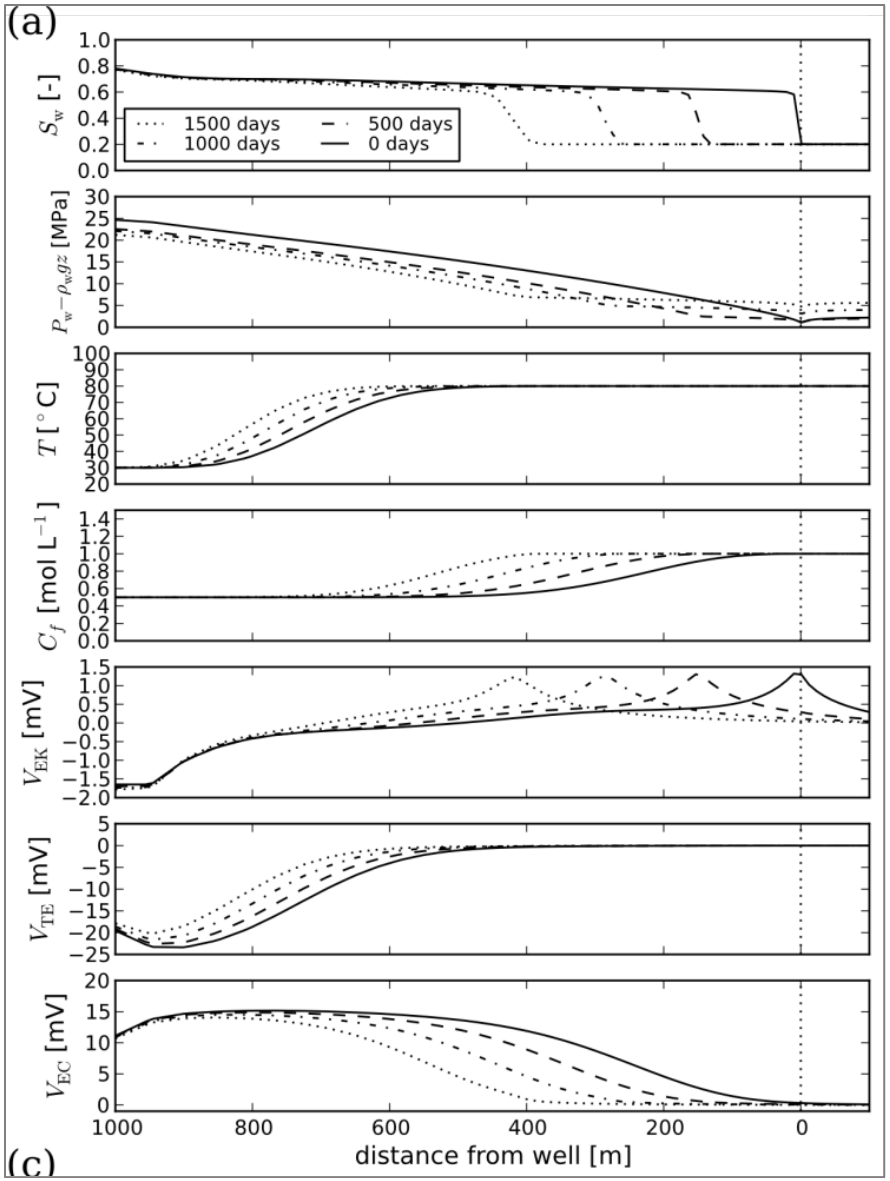

Figure 2. Numerical results from the homogenous reservoir model. Panels show (from top to bottom) brine saturation, water pressure, temperature, salinity, EK, TE and EC potential, as a function of distance from the production well (marked by the vertical dotted line) along a 1D profile through the center of the model, at four different time steps (annotated as time until water breakthrough).

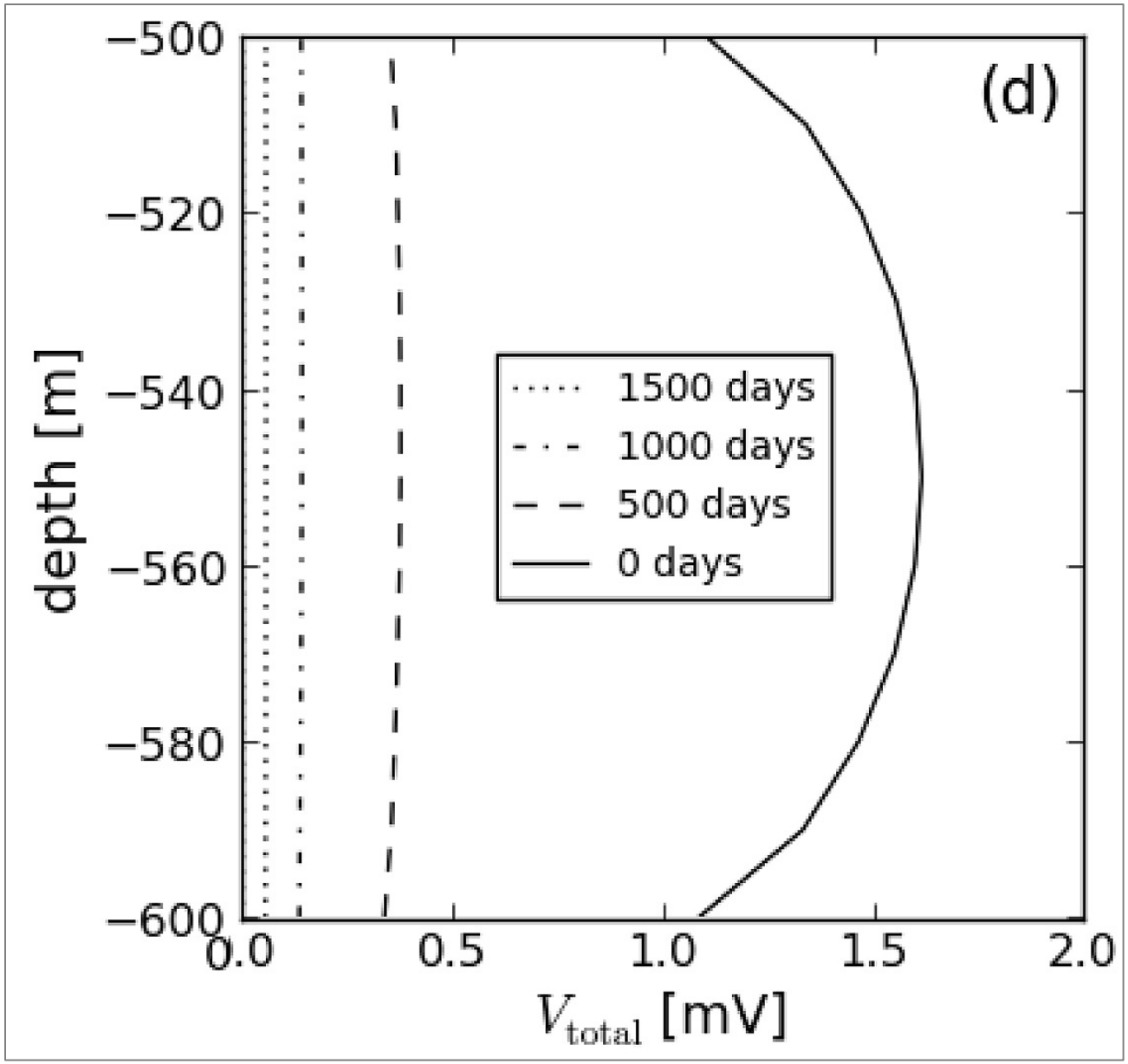

Figure 3. Total SP potential as a function of depth along the production well, at four different times before water breakthrough. Lines styles and simulation times shown are consistent with Figure 2.

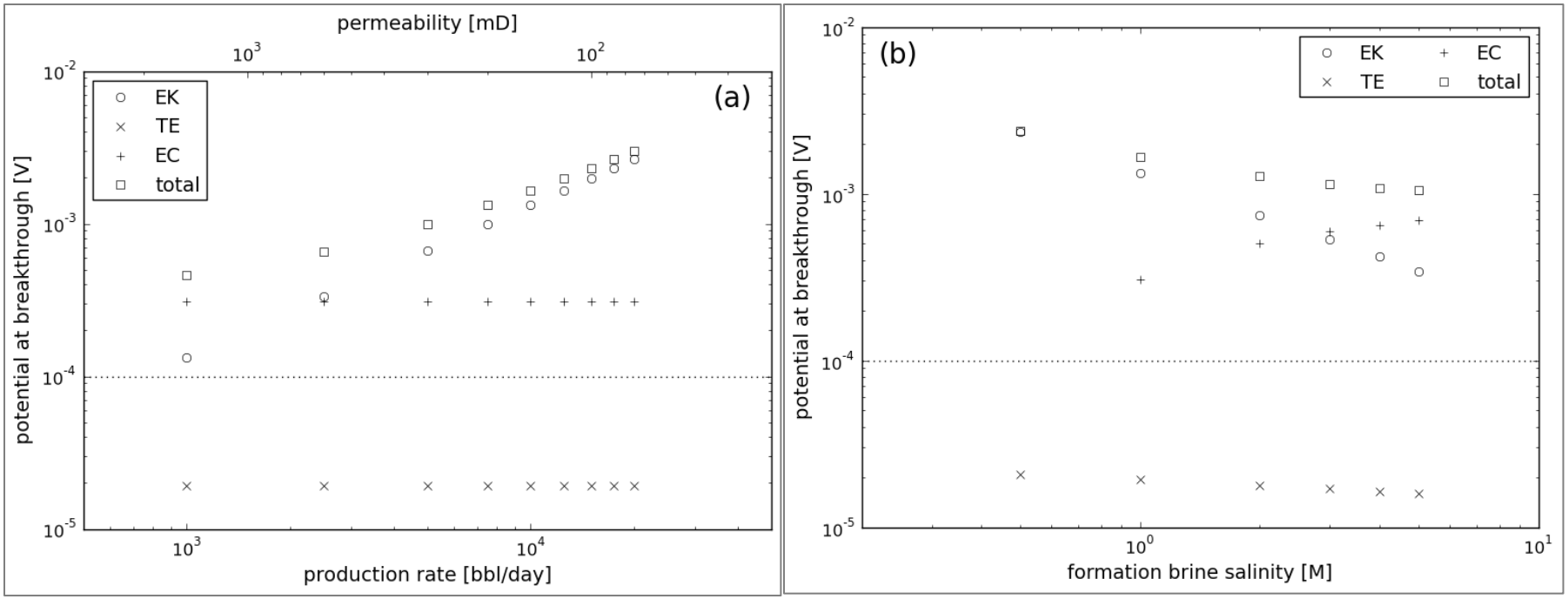

Figure 4. EK, EC, TE and total SP signal at the center of the production well at water breakthrough. The production rate is 10,000 bbl/day, the reservoir permeability is 150 mD, the formation brine salinity and temperature are 1 M and 80° C respectively and the injection brine salinity and temperature are 0.5 M and 30° C respectively, except when they are varied to investigate the effect of (a) production rate and reservoir permeability, and (b) formation brine salinity. The estimated downhole noise level of 0.1 mV is shown by the dashed line.

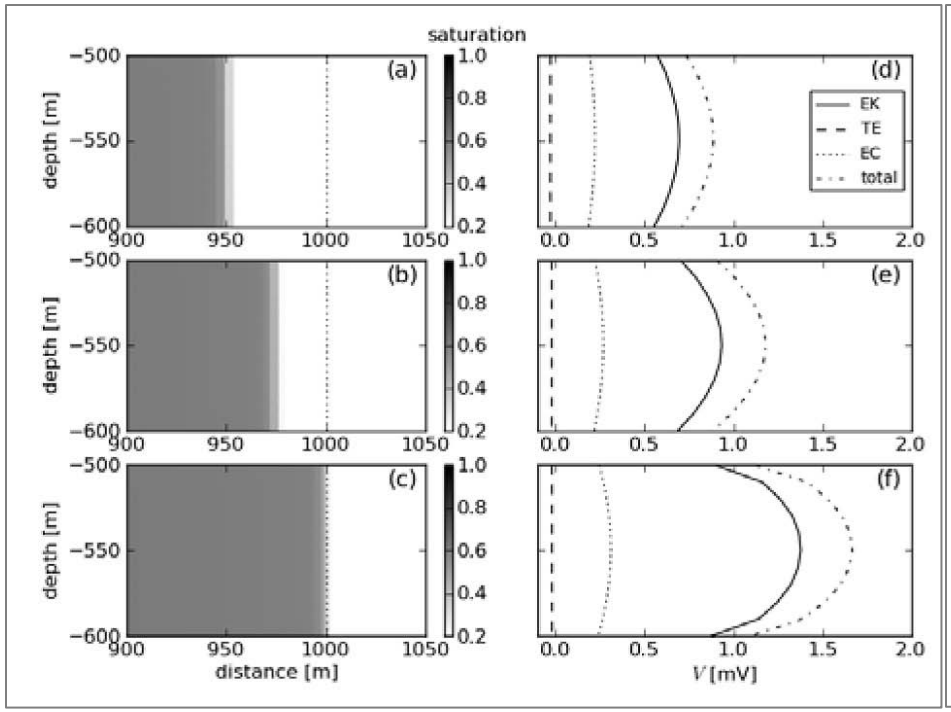

Figure 5. Cross-section through the homogenous model showing water saturation when the waterfront is (a) 50 m away from the production well, (b) 25 m away, and (c) at breakthrough. The well is shown by the vertical dashed line. (d)-(f) Corresponding potentials recorded along the well.

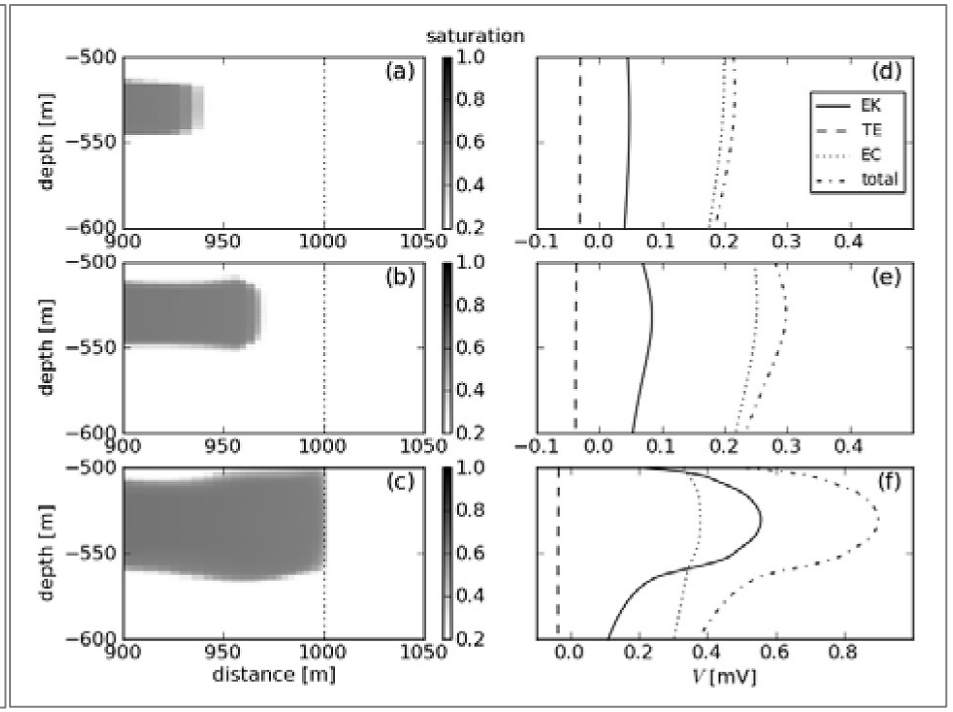

Figure 6. Cross-section through the heterogeneous reservoir model showing water saturation when the waterfront is (a) 50 m away from the production well, (b) 25 m away, and (c) at breakthrough. The well is shown by the vertical dashed line. (d)-(f) Corresponding potentials recorded along the well.